Dynamic processes during displacement cascades in oxide glasses: A molecular-dynamics study

J.-M. Delaye and D. Ghaleb
Commissariat à l'Énergie Atomique (CEA), Rhône Valley Research Center, DCC/DRRV/SCD/LEAM, BP 171, 30207 Bagnols-sur-Cèze Cedex, France

(Received 27 August 1999; revised manuscript received 10 February 2000)

Management of long-lived radioactive nuclear waste implies understanding its structural behavior when subjected to irradiation. This paper presents molecular-dynamics simulations about the effect of a recoil nucleus on a simplified nuclear glass containing SiO_2, B_2O_3, Na_2O, Al_2O_3, ZrO_2 and a few heavy ions of uranium. A statistic on displacement cascades at energies ranging from 300 eV to 7 keV in glass compositions with and without alkali metals revealed the influence of the latter on the thoroughness of structural restoration. More generally, following a depolymerization peak, the glass structure is reconstructed by local readjustments, facilitated by the presence of alkali metal atoms. If the cascade energy is sufficiently high, the initial structure is completely restored. The large majority of the atom displacements occur during the first instants of the cascade, during the thermal peak; displacements during the initial structure restoration phase account for only a small fraction of the total. Several types of displacements were identified, ranging from jumps by individual atoms to collective displacements of an atom and its neighbors. Individual displacements and $O_{bridging}$-$O_{nonbridging}$ transitions were the most numerous during the first instants of the cascade, but were quickly superseded by collective displacements and local break-and-rebranch processes. The structure volume was observed to remain stable or increase after irradiation, but never to diminish. Coincidental evidence was noted between the coordination numbers, the ring size distributions, the Voronoï volumes, and the cell expansion, to provide some lightening about the swelling origin observed experimentally. Finally, we observe the ease with which the nuclear glasses withstand displacement cascades, and this is an important result in regard to the long term storage of the oxide matrices.

INTRODUCTION

The containment of long-lived radioactive waste (actinides and fission products) in oxide glass matrices raises a number of issues related to the types of radiation ($\alpha\beta\gamma$) and the complexity of the matrix, which includes some thirty components (see Ref. 1 for a detailed description of the French nuclear glass called R7T7 glass). Predicting the long-term evolution of the matrix implies understanding its structural behavior when subjected to irradiation.[2]

This article focuses on the behavior of two different oxide glass compositions—with and without alkali metals—subjected to the passage of a recoil nucleus of the type emitted by α decay reactions. One simplification step assumes that the effects of the recoil nucleus and of the α particle are dissociated. We are only interested here in the first phenomenon, which produces the most atom displacements.[3] Molecular dynamics is an effective method for analyzing such events, as shown by numerous published studies mainly involving metals, but also semiconductors and oxides.[4–6] The importance of properties such as the melting temperature or the crystallographic structure has been reported.[7] However, the disordered macrostructure of glass, the combination of species with differing mobility, and the peculiar effects of oxygen anion ''binding'' between cations are distinctive features of oxide glasses that have received little attention to date.

Molecular dynamics[8] is ideal for this purpose. The size of the displacement cascades produced by heavy nuclei is measured in tens of nanometers, and the recoil nucleus energy dissipation time in tens of picoseconds. Both of these orders of magnitude are compatible with the current state of classic molecular dynamics. The relatively simple physical principles behind classic molecular dynamics require the recoil nucleus to be considered as purely ballistic, with no allowance for the electron excitation effects (which would require additional calculation of the electronic structure of the simulated material). Energy losses by electron excitation are estimated at around 15% of the total energy.

Unfortunately, the actual energy of the recoil nuclei range from 70 to 100 keV, and are thus beyond the capacity of existing computer resources. The higher damage energies are doubly penalizing: not only must the size of the simulation cells be increased to match the increased volume of the damage zone, but also the duration of the simulation must be extended to cover the greater time necessary for completion of the dynamic processes initiated by a higher energy nucleus. The maximum energy cascade presented here therefore does not exceed 7 keV.

Complex glass compositions must also be simplified for proper simulation at both a qualitative level (the behavior of each component) and a quantitative level (recoil nucleus effects). Broadly speaking, the glass matrix constituents can be classified in four categories:[9,10] ''hard'' network formers, including silicon atoms for which the local environment is constant from one site to another (a tetrahedron formed by four oxygen atoms); ''soft'' formers such as boron, which oscillate between two perfectly defined types of local environment (oxygen triangle or tetrahedron); intermediate species (Zr, Pu, Fe) whose local environments are subject to greater

TABLE I. Simulated weight percentage compositions, with number of atoms N for each composition ppm of UO_2 corresponds to 2 uranium atoms among 82944 atoms.

SiO_2	B_2O_5	Na_2O	Al_2O_5	ZrO_2	UO_2	N
70.0	30.0	0.0	0.0	0.0	0.0	5184
59.1	18.3	12.8	6.3	3.5	0.0	5184
58.4	18.1	12.7	6.2	3.5	1.1	5184
56.1	17.1	12.3	6.1	3.5	0.0	41972
56.1	17.1	12.3	6.1	3.5	ppm	82944

deformations as reflected by the greater distributions of first-neighbor distances and local coordination numbers; and finally network modifiers such as the alkali metals and the alkaline-earth elements, the least ordered elements with what appears to be a continuous, uncountable range of local environments. Oxygen atoms, the only anions in R7T7-type nuclear oxide glasses, ensure cohesion between the various categories of cations. This arbitrary classification reflects the large variety of glass constituent elements, which probably covers the entire range of possible local order levels rather than these four schematic categories.

In the simulated glass compositions, we have included species from each of these categories in proportions corresponding to the actual composition of the complex R7T7 glass. This procedure was adopted to assess the specific influence of the elements, according to their level of local order, on the displacement cascade sequence, on the dynamic processes characterizing the cascade, and on the resulting structural modifications. Cascades with energies above 1 keV were simulated in 5-oxide glasses with larger cells (41472 and 82944 atoms) using a parallel processor computer ($T3E$); the scope of the statistical coverage was limited by the high cost of this approach.

METHODOLOGY

Glasses of various sizes and compositions (Table I) were prepared by combining the algorithms in NVE (constant number of atoms, volume, and energy) and NPH (constant number of atoms, pressure, and enthalpy) systems. The initial volume was determined by a phenomenological model validated over a wide range of glass compositions.[11] An initial liquid phase was prepared for ten thousand 10^{-15} s time steps by stabilizing the initially random configuration between 5000 and 6000 K. As soon as the temperature exceeded 6000 K, the atom velocities were reequilibrated at 5000 K. The second step involved rapid quenching at a rate of $10^{15}\,\mathrm{K\,s^{-1}}$ until 2000 K and subsequently $4\times10^{14}\,\mathrm{K\,s^{-1}}$ below 2000 K to obtain a vitreous structure at room temperature. A constant-pressure algorithm[12] (NPH thermodynamic system) was then applied to determine the exact equilibrium volume in five thousand 10^{-15} s time steps. The final 10000-step relaxation was applied in the NVE system by setting the system volume to the previously calculated equilibrium value.

Classic oxide glass interaction potentials were used. These Born-Mayer-Huggins potentials represent ionic and covalent interactions by the sum of two terms: Φ_2 pairs and Φ_3 three-body terms. The analytical form of the three-body terms was developed by Stillinger and Weber,[13] but the SiO_2 parameter values were determined by Feuston and Garofalini:[14]

$$\phi_2(r_{ij}) = A_{ij}\exp\left(-\frac{r_{ij}}{\rho_{ij}}\right) + \frac{z_i z_j}{r_{ij}}, \tag{1}$$

$$\phi_3(r_{ij}, r_{ik}, \theta_{jik}) = \lambda_i \exp\left(\frac{\gamma_i}{r_{ij}-r_{ci}} + \frac{\gamma_i}{r_{ik}-r_{ci}}\right) \times (\cos\theta_{jik} - \cos\theta_0)^2, \tag{2}$$

where z_i and z_j correspond to the charges of the interacting atoms i and j; $r_{ij}(r_{ik})$ is the distance between atoms i and j (i and k); A_{ij} and ρ_{ij} are two adjustable parameters of the pair terms; the atom at the center of the ijk triplet in the three-body terms is subscripted i, and the outer atoms j and k; θ_{jik} is the angle formed by the triplet; λ_i and γ_i are adjustable parameters depending on the chemical nature of atom i. The parameter values are indicated in Table II and Table III.

TABLE II. Adjustable parameter values A_{ij} (eV) for Born-Mayer-Huggins potentials $\rho_{i\text{-}j} = 0.29$ Å (except $\rho_{o\text{-}o} = 0.35$ Å).

Species	Si	O	B	Na	Zr	Al
Si	834.4	1571.2	337.7	862.0	2557.4	961.3
O		352.68	760.9	1396.4	4805.2	1734.0
B			121.1	374.5	1031.8	396.4
Na				842.1	2637.9	976.3
Zr					7822.7	2940.7
Al						1100.5

These parameters are either based on earlier work with simpler oxides, or were readjusted for complex glasses to account for their structure and various macroscopic properties.[15,16] Short-range interactions (less than 0.9 Å) occurring during the cascades were modeled by the Ziegler-Biersack-Littmark potential[17] and related to the Born-Mayer-Huggins terms (above 1 Å) by fifth-order polynomial expressions.

The first molecular dynamics calculations in oxides showed that pair terms alone could not correctly account for the local order around the formers, hence the idea of using higher-order corrective terms.[13,14,18–20] Using formal charges to represent Coulomb interactions may seem to be an aggressive hypothesis, but while with simple oxides the potential formulas and charge values can be polished to obtain a very accurate representation of the structure and physical properties of the material, with a mixture of oxides the use of partial charges becomes problematic: the different cation electronegativity values result in charge transfers of different intensity depending on the chemical nature of the bonds.

TABLE III. Adjustable parameter values λ_i (eV), γ_i (Å), and θ_0 for three-body terms.

Parameter	O-Si-O, O-Al-O	Si-O-Si	O-B-O
λ_i (eV)	149.8	6.2	11985.0
γ_i (Å)	2.6	2.0	2.27
θ_0	109.47°	160.0°	109.47°

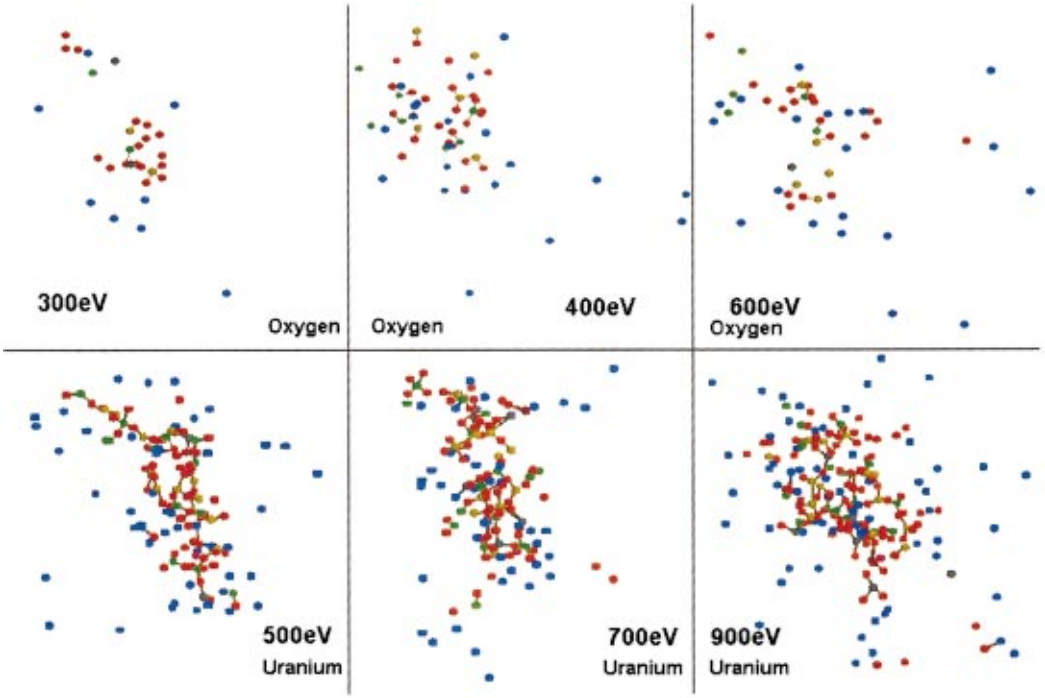

FIG. 1. (Color) Morphology (displaced atom positions) of six cascades in a 5184-atom alkali glass (see composition in Table I). Si(yellow), O(red), B(green), Na(blue), Zr(brown), and Al(gray).

Imposing one of the charges on a type of ions mechanically imposes the other ion charge values because of the overall electroneutrality requirement. With highly covalent formers and highly ionic modifiers, no satisfactory tradeoff is possible. We therefore chose to use formal ionic charges; the corrections necessary to take into account the varying degree of covalence of certain chemical bonds are modeled using three-body terms.

In the glass analyses with 82944 atoms, a few U^{4+} ions were added to simulate cascades initiated by heavy particles.

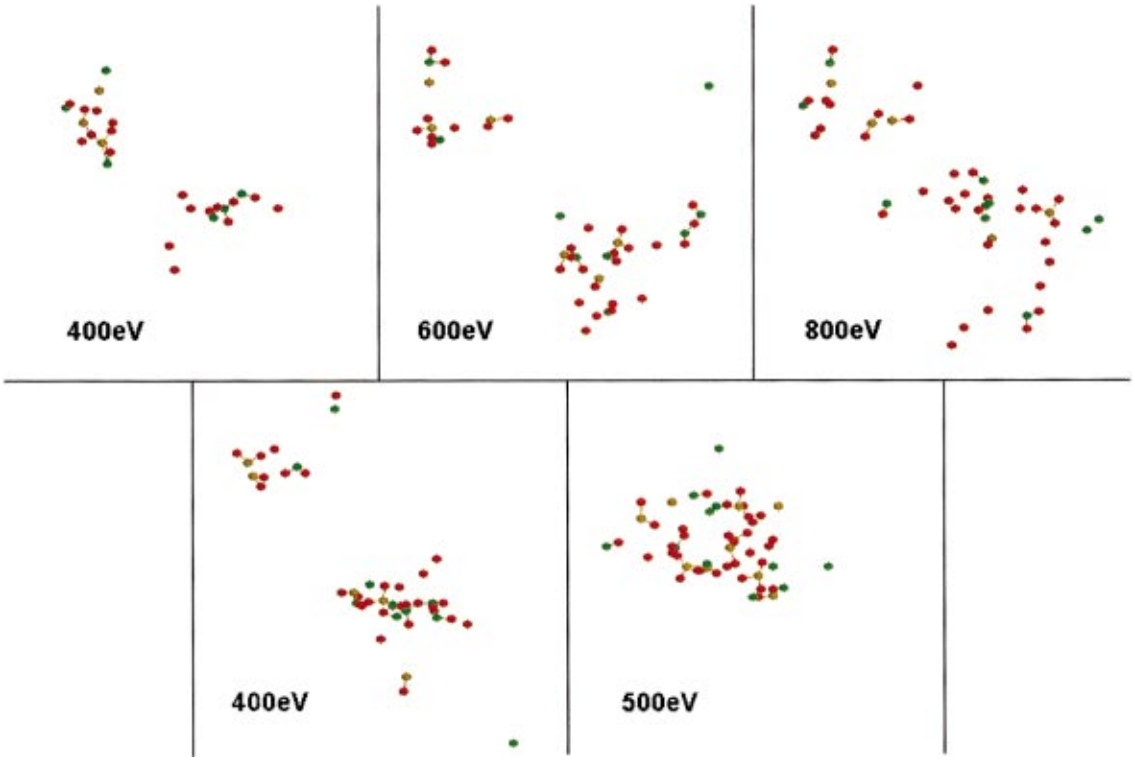

FIG. 2. (Color) Morphology (displaced atom positions) of five cascades in a 5184-atom alkali-free glass (see composition in Table I). These cascades are initiated by O atoms. Si(yellow), O(red), and B(green).

U-O interactions were modeled by the potential developed by Lindan *et al.*[21] while U-cation interactions were assumed to be purely Coulombian.

A displacement cascade of energy E and direction ϵ was initiated by adding an atom with a kinetic energy E and a kinetic moment in direction ϵ to reproduce the effect of an elastic collision between the atom and a particle of undetermined nature. This technique has been described in detail by Doan and Rossi.[22]

Because of the high initial atom velocities, the time step was reduced to 10^{-17} s at the beginning of the cascade to prevent the maximum displacement of any atom from exceeding 0.01 Å per time step (an empirical tradeoff between the energy conservation requirement and a reasonable calculation time). As the kinetic moment of the projectile was then distributed over the atoms in the glass matrix, the maximum atom velocity diminished and the time step was increased accordingly: 5×10^{-17} s, then 10^{-16} s and finally 10^{-15} s. The time steps were modified by means of a third-order motion equation in which the new atom positions were calculated from the previous positions and atom velocities:

$$\mathbf{X}(t)=\mathbf{X}(t-\delta t)+\delta t\times\mathbf{V}(t-\delta t)+\frac{\delta t^2}{2m}\mathbf{F}(t-\delta t). \quad (3)$$

The simulation cell was gradually cooled to room temperature by controlling the outer layer. The atom velocities in the outermost 3.5 Å were periodically reequilibrated to room temperature using the classic equation: $3/2kT=1/2mv^2$. As soon as the thermal wave reached the outer limits of the cell, it was thus dissipated as if the glass were in thermal contact with a room-temperature bath.

Cascades at energies between 300 eV and 2.0 keV were initiated by accelerating an oxygen or an uranium atom; only uranium atoms were used for energies above 3 keV. The displacement cascades were simulated in the NVE system. Although the damage zones were submitted to intense intermediate pressure peaks, the pressure was not at equilibrium and varied significantly from one point to another in the simulation cell. It was therefore impossible to use a constant-pressure algorithm based on continuous reequilibration between the assumed equilibrated internal pressure and an imposed external pressure.

The effects of a projectile on the glass were quantified at atomic scale according to the number of displacements, the polymerization level of the glass structure, and globally based on expansion of the simulation cell. An atom was empirically defined as ''displaced'' if its path during the cascade exceeded 1 Å (i.e., exceeded an energy barrier). The depolymerization level N_{poly} was defined as follows:

$$N_{\mathrm{poly}}(t)=\sum_{i=\mathrm{Si,O,B,Al}} N_c(i,0)-N_c(i,t), \quad (4)$$

where $N_c(i,t)$ and $N_c(i,0)$ represent the atom coordination numbers at time t and at the cascade initiation time 0. In other words, the instantaneous numbers were compared with the initial chemical bonds, and the difference between them corresponded to the number of bonds broken by the projectile. Only network formers and oxygen atoms were taken into account in calculating the depolymerization level.

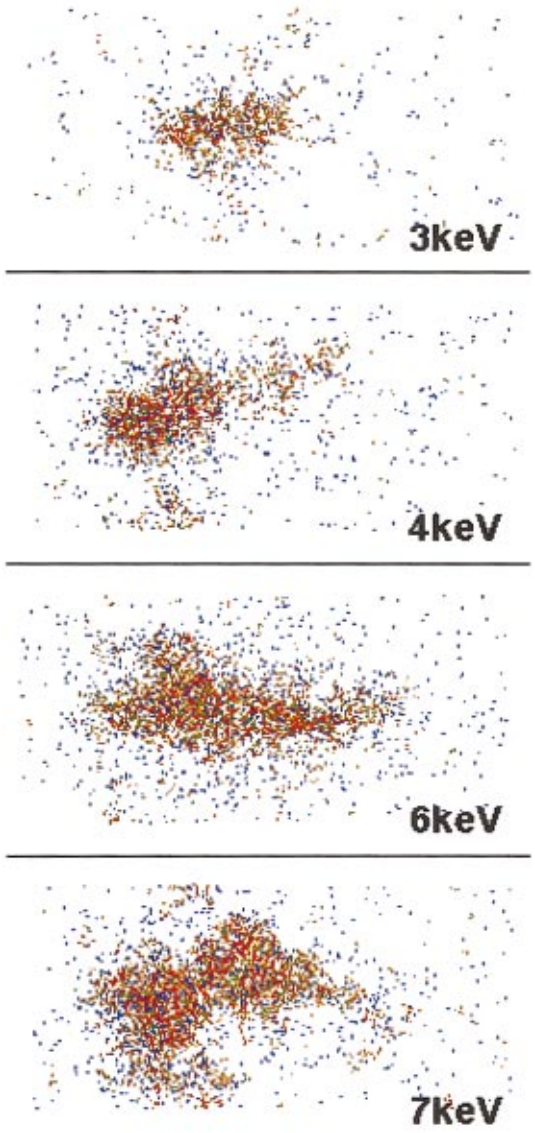

FIG. 3. (Color) Morphology (displaced atom positions) of four cascades in a 82944-atom alkali glass (see composition in Table I). These cascades are initiated by U atoms. Si(yellow), O(red), B(green), Na(blue), Zr(brown), and Al(gray).

Expansion was measured after the cascade either by recalculating the final equilibrium volume of the simulation cell or by measuring the internal pressure change according to Viriel's theorem after the passage of the projectile, and estimating the expansion from the compressibility modulus.

RESULTS

Displacement cascade morphology

Figures 1 and 2 show several damage zone morphologies at various energies in 5184-atom cells with and without alkali metal atoms. In this paper, the term morphology refers to the positions of the displaced atoms. Typical morphologies of cascades with energies exceeding 3 keV in 5-oxide glasses with 82944 atoms are plotted in Fig. 3. Each image shows only the atoms displaced by more than 1 Å between the initial and final instants of the cascade. Displaced close-neighbor atoms are shown linked together.

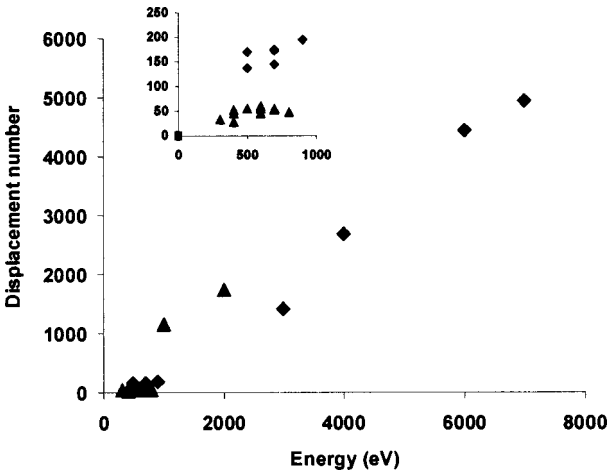

FIG. 4. Number of atom displacements versus cascade energy. Cascades initiated by (♦) U atoms and (▲) O atoms.

Some of the damage zones can be seen to include highly disturbed regions containing numerous atom displacements, and other only lightly disturbed regions. No glass composition effect can be clearly established from these figures. Conversely, as the energy increases the distinction between the damage regions tends to disappear in both compositions (with and without alkali metal). The three images at the top of Fig. 2 correspond to cascades of 400, 600, and 800 eV in an alkali-free glass initiated by the same oxygen projectile in the same direction; the second and fourth images of Fig. 3 represent cascades of 4 and 7 keV, again initiated by accelerating the same uranium projectile in the same direction. The mechanism of this disappearance involves the growth of each of the subregions, which tend to overlap.

The damage zones are situated for the most part along the projectile path. Subcascades initiated by a secondary atom ejected by a collision with the projectile begin to appear only in cascades exceeding 3 keV, and are often interrupted by the temperature control at the simulation cell boundaries. Nevertheless, these subcascades represent a small fraction of the total morphology, and there is no effect on the structural relaxation as we will see below.

Another phenomenon related to increasing energy in the alkali-free glass is visible in the number of displaced polymerized chains. The latter are found in greater numbers at lower energies (see the cascades at 400 and 500 eV), but become less frequent at higher energies (600 and 800 eV). The atoms displaced in the last two examples appear more isolated than for the low-energy cascades.

In glass compositions containing alkali metals, it is interesting to note that each damage zone is surrounded by a multitude of alkali metal atoms, although this does not imply that the displaced alkali metals are absent from the center of the disturbed regions. Medium-range sodium atom displacements are also routinely observed outside the disturbed regions. When the projectile is an uranium, the morphologies are more dense along the path.

TABLE IV. Elementary cell occupation. The number of cells containing 80% of the displacements is indicated in column 2, and the mean cell occupation in column 3.

Energy	Number of cells	Mean occupation
3 keV	456	2.5
4 keV	855	2.51
6 keV	1148	3.09
7 keV	1169	3.39

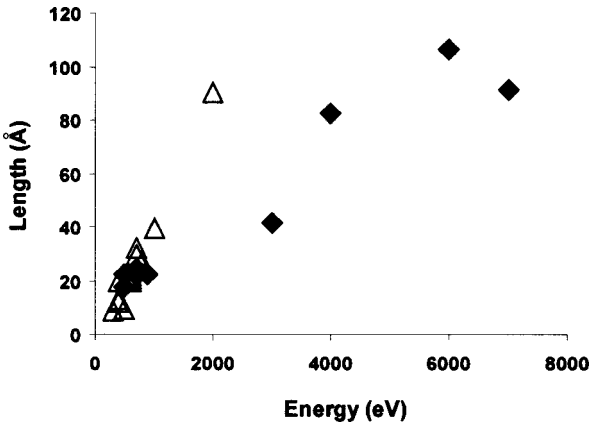

FIG. 5. Initial projectile path length versus energy. Cascades initiated by (♦) U atoms and (△) O atoms.

We plotted the number of displacements versus the cascade energy, using different symbols to identify the projectiles and simulation cell dimensions (Fig. 4). The slope of the trend line followed by the low-energy data points is significantly lower than for the high-energy points. The inset in Fig. 4 shows that in the 5184-atom cells, an accelerated U atom provokes a number of atom displacements larger by a factor about 3. This phenomenon does not occur at higher energies in the larger cells: the cascades at 1 keV and 2 keV (initiated by O atoms) are on the same line as the points corresponding to cascades initiated by U atoms. The method used to cool the simulation cell during the cascades affects the number of atom displacements (refer to the discussion below).

We estimated the atom displacement density in the damage zones for the high-energy cascades as follows. The 82944-atom cell was subdivided into 13718 unit cells within which the number of displaced atoms was measured. The mean number of displacements per cell was then calculated for the most occupied unit cells, containing 80% of all the displacements. This approach eliminated the marginal cells with few displacements or situated far from the center of the irradiated zone.

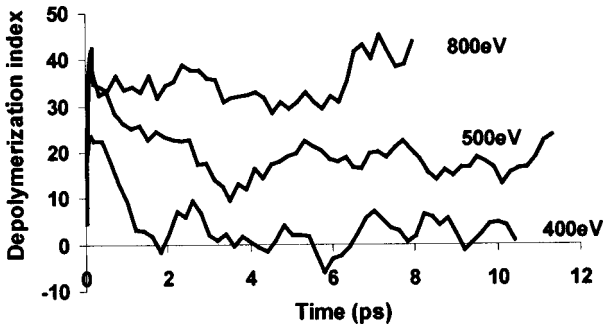

FIG. 6. Three typical depolymerization versus time curves for a 5184-atom alkali-free glass.

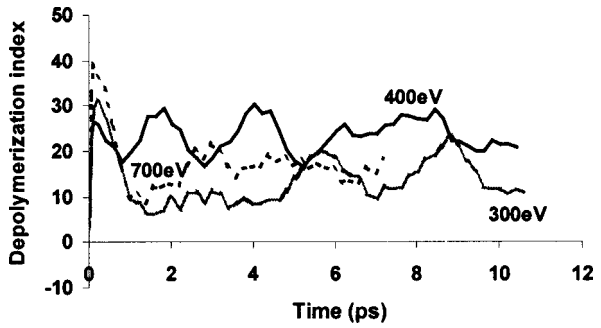

FIG. 7. Three typical depolymerization versus time curves for a 5184-atom alkali glass.

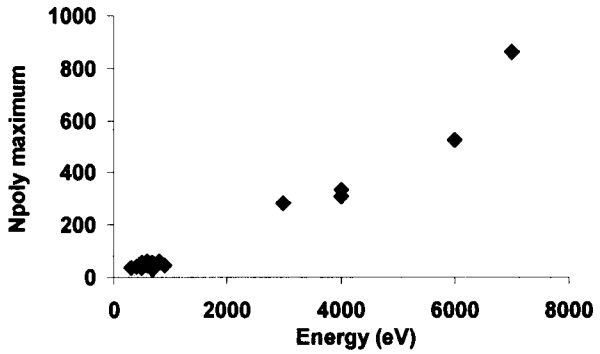

FIG. 9. Maximum depolymerization peak versus energy.

Table IV indicates the number of unit cells considered for the four cascades with the highest energies, and the mean occupation of each cell. The number of unit cells increased with the cascade energy, reflecting the energy-dependent increase in the spatial coverage of the cascades; the higher mean occupation is attributable to the higher displacement density.

Figure 5 shows the projectile path length versus energy for glass compositions with and without alkali metals. The lengths are equal to the norm of the vector between the initial and final projectile positions, with no allowance for possible path curvature (the visual curvature was small in every case). There is a linearity between the path distance and the energy but with a slope depending on the nature of the projectile. The lighter O atoms have longer path distance than the heavier U atoms. Conversely, the continuity between the calculated data points in the 5184-atom cell and those in the larger cells shows that the phenomenon responsible for the change in slope of the number of displacements has no effect on the path distance.

At low energies, the overlap of the data point arrays for compositions with and without alkali metals (not separated on the figure) indicates that there is no obvious composition effect on the initial projectile path length.

Depolymerization in time

The curves in Figs. 6, 7, and 8 show the typical evolution in time of the depolymerization levels defined by Eq. (4) for various cascades. The same behavior can be observed in each case for the glasses containing an alkali metal: the depolymerization index rises quickly during the initial instants, then, with a longer characteristic time, the structure gradually returns toward the initial polymerization level. In practically no case does the system finish in a state of greater polymerization than at the outset: either some degree of depolymerization remains, or the system reverts to its initial polymerization state.

In the alkali-free glass, the repolymerization phase is less pronounced, and sometimes absent.

The height of the initial depolymerization peaks is plotted versus the projectile energy in Fig. 9, which shows a linear increase with energy throughout the range from 0 to 7 keV. Here again, the low-energy limitation on the number of displacements is not applicable.

Figure 10 plots the final depolymerization (calculated by averaging the final part of the curve) versus the ratio between the cascade energy and the number of atoms in the cell. Different symbols are used to indicate the presence or absence of alkali metals, and clearly reveal the different behavior of the two types of glass. The final depolymerization increases with the deposited energy for the alkali-free glass, and diminishes for the alkali glasses; this phenomenon reflects the ease of restoring the structure when the glass contains alkali metals. The points corresponding to cascades in a 82944-atom cell are also plotted for information, but there is no possible quantitative comparison between simulation cells with different dimensions.

The structural depolymerization corresponds to changes in the coordination numbers of each species. Figure 11 shows the number of coordination transitions versus time for

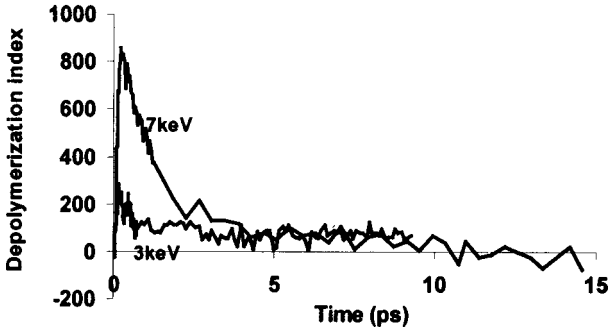

FIG. 8. Two typical depolymerization versus time curves for an 82944-atom alkali glass. Note that oscillation frequencies are different because the depolymerization level is calculated with a shorter period for the 3 keV cascade.

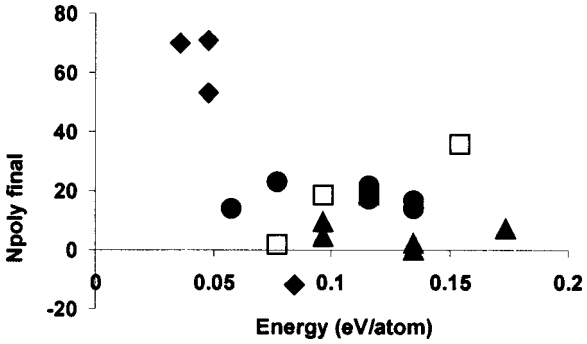

FIG. 10. Final depolymerization versus ratio of energy to atom number in the simulation cell. Calculations for an alkali-free glass (□), U accelerated in a 82944-atom cell (♦), U accelerated in a 5184-atom cell (▲), and O accelerated in a 5184-atom cell (●).

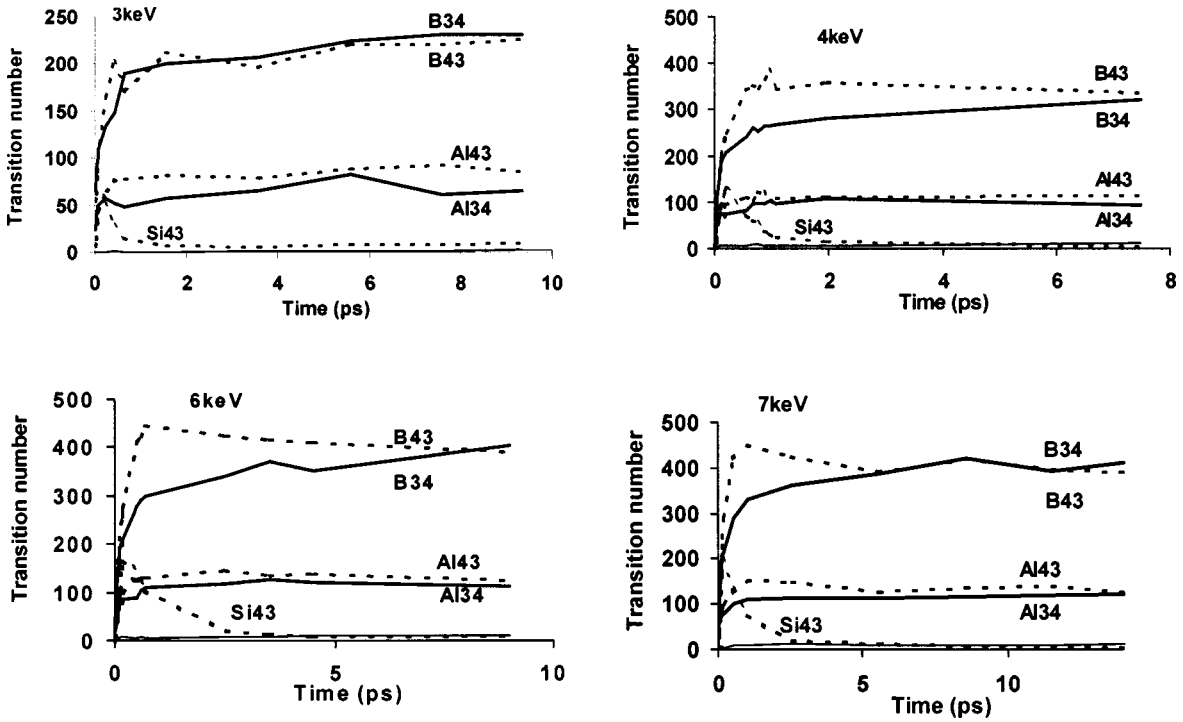

FIG. 11. Number of A_{lm} transitions versus energy for four cascades in an alkali glass. See text for the definition of A_{lm}.

the network formers Si, B, and Al during cascades at energies exceeding 3 keV (A_{lm} corresponds to the number of transitions of cation A from the l-coordinate to the m-coordinate state). The SiO_4 tetrahedrons are restored very rapidly. Boron and aluminum, on the other hand, may belong to two different types of groups. The continuous rise to saturation of the curves representing transitions around boron and aluminum atoms shows that these transitions are irreversible: the boron and aluminum atoms that sustain a local structure transition conserve their new state until the end of the cascade. Moreover, the time necessary to restore the initial group type densities corresponds to a longer-term relaxation of the glass structure, unlike the very rapid restoration of the SiO_4 tetrahedrons.

The evolution in time of the number of transitions from two-coordinate to one-coordinate oxygen and vice versa is

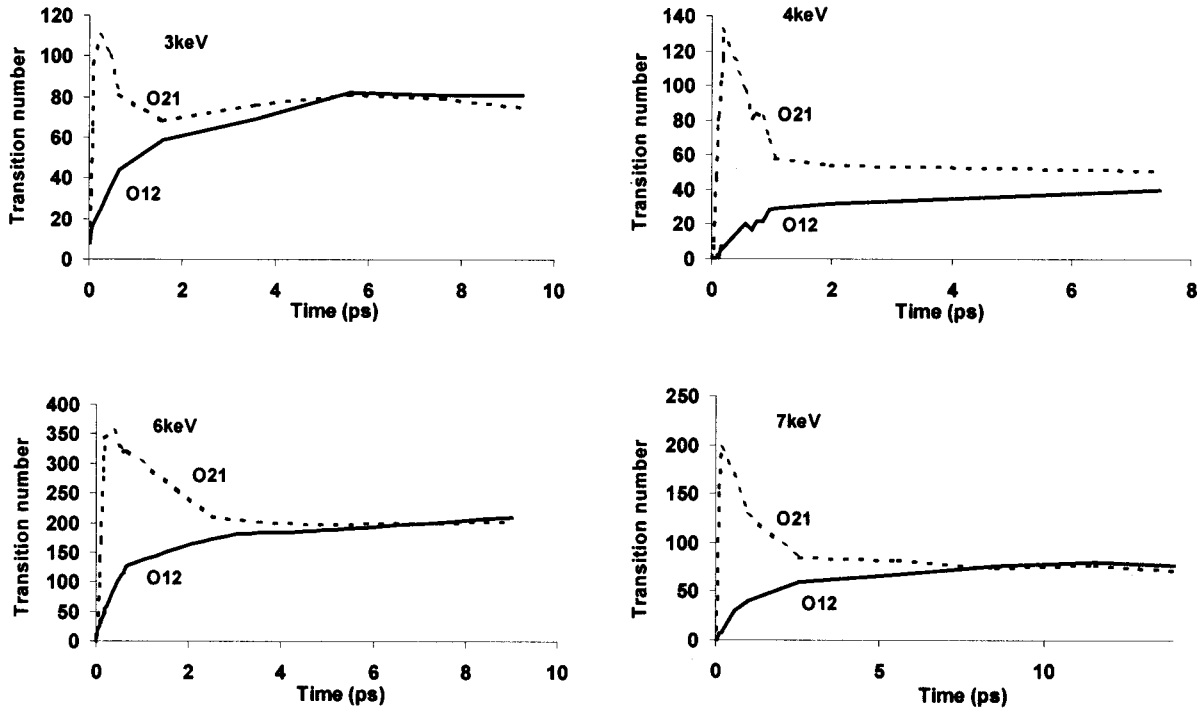

FIG. 12. Number of O_{12} ($O_{nonbridging} \rightarrow O_{bridging}$) and O_{21} ($O_{bridging} \rightarrow O_{nonbridging}$) transitions versus energy for four cascades in an alkali glass.

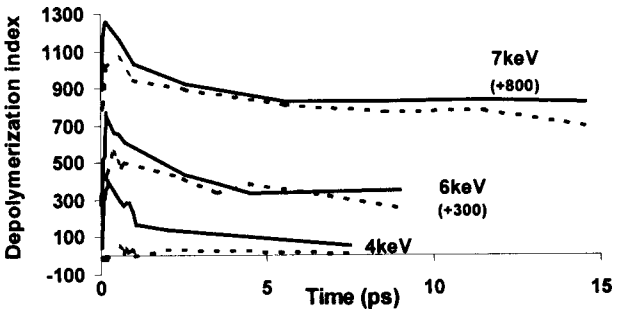

FIG. 13. Depolymerization index versus time for three cascades in an alkali glass. Solid curve: initial damage zone; dotted curve: second damage zone (refer to text for explanation). Curves are shifted (offset indicated in parentheses).

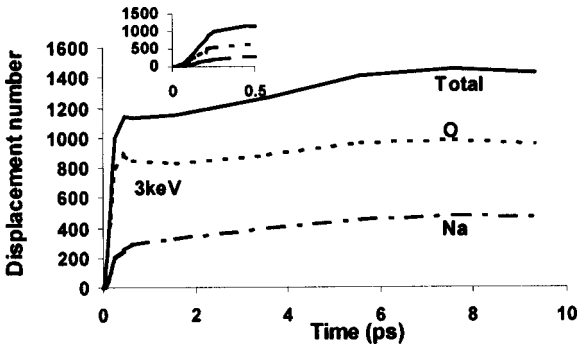

FIG. 14. Number of displaced oxygen and sodium atoms and total number of atom displacements versus time for a 3 keV cascade in an alkali glass (inset: enlargement of 0–0.5 ps region).

plotted in Fig. 12. The initial depolymerization peak is clearly correlated with the creation of nonbridging oxygen atoms. A progressive relaxation then occurs, characterized by the restoration of some bridging oxygen atoms; at the same time, a number of nonbridging oxygen atoms disappear. The end result is to restore the balance between bridging and nonbridging oxygen atoms to its precascade state. The characteristic time required to restore this balance depends on the cascade energy: the O_{12} and O_{21} curves join increasingly early as the energy rises from 4 to 6 to 7 keV. The relaxation time for the 3 keV cascade, on the other hand, was comparable to that of the 7 keV cascade. The damage zone morphology may account for this effect: the subdivided morphology created by the 7 keV cascade could impede the structural restoration compared with the homogeneous morphology of the 3 keV cascade.

For the 4, 6, and 7 keV cascades, we roughly delimited the two largest disturbed regions and calculated the polymerization changes over time in each of them (Fig. 13). For all three cascades, the highest depolymerization peak was always observed in the zone disturbed initially. The second zone showed virtually no depolymerization during the 4 keV cascade, while for the 6 and 7 keV events the second region affected by the initial projectile showed the initial stages of depolymerization. In all three cases, the maximum depolymerization peak in the initial zone reached a similar height—about 400—and the differences in the disturbed regions appeared only thereafter.

Types of atom displacement

We examined the total number of displacements over time, and the displacements for each species. A typical example of a 3 keV cascade in a 5-oxide glass is shown in Fig. 14. In percentage terms relative to the atomic composition, the alkali metals clearly account for the largest number of displacements; among the network formers, boron is displaced more than silicon. In percentage terms relative to the total number of displacements, sodium and oxygen account for about 75% of the displacements, with significant difference from one cascade to another. Sodium atoms accounted for between 25% and 50% of the total displacements. These results are observed whatever the nature of the projectile.

The enlarged inset in Fig. 14 covering the 0–0.5 ps time range reveals a slight delay (estimated at about 10^{-13} s) in the displacement of the sodium atoms compared with the other species. This phenomenon is discussed below, in conjunction with the peripheral location of the sodium atoms in the displacement cascade morphology.

The presence or absence of alkali metals had no significant effect on the distribution of the displacement lengths (not indicated in this article).

Comparing the curves plotting the number of displacements versus time with the depolymerization curves shows that the vast majority (about 90%) of the displacements occurred during the first depolymerization peak—i.e., between 0 and 0.5 ps. This observation implies that the reconstruction of the glass structure occurring after 0.5 ps represented only a small portion of the atom displacements.

We analyzed the displacement modes of the oxygen atoms with respect to their local environments during the cascade. Almost all oxygen displacements can be considered in one of the following four mutually exclusive categories: individual displacements during which all the oxygen neighbors are changed; displacements related to a change in the coordination number (conversion from bridging to nonbridging oxygen or vice versa, or from 3-coordinate to 2-coordinate oxygen and vice versa) with conservation of the neighbor atoms of the lowest coordination state; collective displacements during which the identities of the neighboring atoms are unaffected; intermediate events in which part of the neighboring atoms are modified without any change in the oxygen coordination number (this type of displacement involves breaking a bond and ''rebranching'' to another network former).

The percentages of each displacement type evolve over time according to a consistent pattern. A typical 3 keV cascade is shown in Fig. 15. Only the O_{21} transitions (the majority) are shown for the second displacement category. Each point includes all the intervening displacements since the beginning of the cascade. Two distinct regimes can be observed. First, individual and coordination-change displacements rise to a maximum, after which collective displacements and local ''break & branch'' processes predominate. At the end of the cascade, the latter account for a large majority of the total displacements.

High-energy collisions occur during the initial instants of the cascade, causing some atoms to be removed from their equilibrium sites. Although no major displacements occur after 0.5 ps, Fig. 11 and Fig. 12 describe the trend of changes in the coordination numbers around network formers and oxygen atoms, showing that the activity continues after the

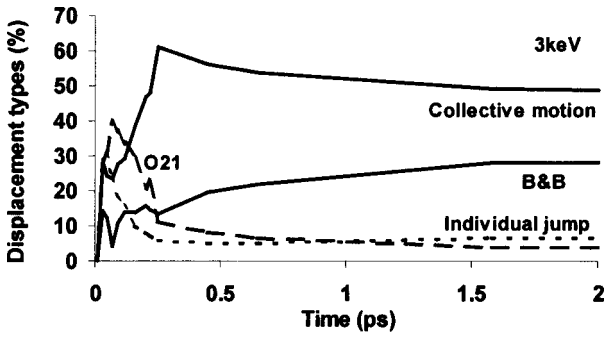

FIG. 15. Percentage distribution of displacements by type (refer to text for definition) for a 3 keV cascade in an alkali glass (''B&B'': break-and-branch processes).

depolymerization peak. The creation of nonbridging oxygen atoms, followed by the reversion to the initial bridging and nonbridging oxygen densities, are by definition related to the presence of alkali metals. The mixture of 1-, 2-, and 3-coordinate oxygens in alkali glasses results in a higher percentage of oxygen affected by a change in coordination than in alkali-free glasses containing no single-coordinate oxygen. These figures reflect the higher local reorganization potential around oxygen atoms when alkali metals are present.

Expansion measurements

Two techniques were used to measure the change in the simulation cell volume after the cascade, as described above under ''Method.'' The pressure variations sustained by the large glass samples during 3, 4, 6, and 7 keV cascades (Table V) reveal a systematic pressure rise after the passage of the projectile, indicating a tendency to swell. Given the bulk modulus (bulk moduli of 117 GPa and 113 GPa were measured in the two 82944-atom glasses) the difference can be converted into an estimated expansion factor; the estimated volume change is also indicated in Table V. The pressure rise diminished as the projectile energy increased, providing further evidence of improved structural restoration at higher energies. We may expect a maximum of the pressure rise for an energy comprised between 0 and 3 keV because obviously for a zero energy cascade, no pressure rise will occur.

A direct calculation (with Andersen's algorithm) of the volume change after the 3 keV cascade confirmed the volume change of 0.26%.

The equilibrium volumes before and after low-energy (<1 keV) cascades were directly compared to obtain the expansion values in Table VI. Here again, the volume change (if any) was limited and systematically positive. Expansion was greater in the SiO_2-B_2O_3 glass, with one strange case in which an 800 eV cascade resulted in appreciable depolymerization, but no volume change.

The origin of the expansion was analyzed for low-energy cascades (<1 keV) and the 3 keV cascade by measuring the

TABLE V. Pressure variations after 3, 4, 6, and 7 keV cascades.

	3 keV	4 keV	6 keV	7 keV
ΔP (GPa)	0.305	0.157	0.123	0.129
$\Delta V/V$ (%)	0.261	0.139	0.109	0.114

TABLE VI. Volume variations in glasses with and without alkali metals. The projectile is an O atom in each case.

W/o alkali	500 eV	600 eV	800 eV	400 eV		
$\Delta V/V$ (%)	0.14	0.30	0.0	0.12		
with alkali	600 eV	700 eV	600 eV	400 eV	300 eV	700 eV
$\Delta V/V$ (%)	0.04	0.02	0.12	0.18	0.05	−0.03

Voronoï volumes of various atomic species and the evolution of the ring size distribution. The percentage variations of the Voronoï volumes for the cascades resulting in the greatest expansion are indicated in Table VII (alkali-free glass) and Table VIII (alkali glass). Expansion in the alkali-free glass was localized in the immediate environment of the boron atoms, mainly due to a coordination effect: the Voronoï volumes of 3-coordinate boron atoms are larger than those of 4-coordinate boron, and the volume increase was due to an increase in the relative number of 3-coordinate boron atoms. In the alkali glass, expansion occurred around boron atoms as well as around sodium atoms, but with fluctuations—notably around aluminum atoms—that will require confirmation by more extensive simulations. The local environments of the silicon atoms remained highly stable in the alkali glass medium and slightly less so without alkali metals, confirming the previously noted stability of the SiO_4 tetrahedron.

It is interesting to observe the dynamic evolution of the ring distributions, and the changes that occur between the initial and final states. For each oxygen atom, we identified the smallest ring (if any) in which it was contained. The statistics were compiled from the set of all these rings, providing an indication of the fineness of the network mesh. Figure 16 shows the evolution of the number of rings during 4 keV and 7 keV cascades; large rings (arbitrarily defined as rings containing more than 6 oxygen atoms, and accounting for about 10% of the total number) are indicated separately to provide a schematic representation of the evolution of the polymerized network during the cascades. The ''large rings'' category exhibited different behavior from that of the small rings. The number of large rings increased following the depolymerization peak, then diminished to its initial value; the reversion to the initial state was more complete at higher energies, while the number of large rings clearly increased after the 3 keV (not shown) and 4 keV cascades. The remaining 90% of ''small'' rings exhibited the opposite behavior: their number diminished with the depolymerization, then rose again to the initial value; incomplete structural relaxation resulted in a deficit in the final number of small rings.

The angular distributions (not shown here) were unaffected in any of the compositions studied. Similarly, the

TABLE VII. Voronoï volume variations (%) for simulated cascades in a $SiO_2+B_2O_3$ glass.

Energy (eV)	$\Delta V/V$ (%)	Si	O	B
500 eV	0.14	0.1672	0.1006	0.3655
600 eV	0.30	0.1987	0.2770	0.6158
400 eV	0.12	0.0274	−0.0946	0.5519

TABLE VIII. Voronoï volume variations (%) for simulated cascades in a five-component glass.

Energy (eV)	$\Delta V/V$ (%)	Si	O	B	Na	Zr	Al
600 eV	0.12	−0.0056	0.0916	0.6780	0.1821	0.0317	−0.8741
400 eV	0.18	−0.0631	0.1531	0.7509	0.1972	−0.0526	0.0066
3 keV	0.26	0.056	0.272	0.452	0.31	−0.01	0.52

number of B-O-B triplets remained globally constant, demonstrating that no detectable segregation of boron atoms occurred in the silicate network.

DISCUSSION

Size effects

The results presented above must be situated within the context of the method used, with due allowance for possible artifacts. In particular, the change in slope observed in the total number of displacements (Fig. 4) when the size of the simulation cell was increased warrants a more detailed analysis.

Figure 17 shows the temperature evolution during cascades in the 5184-atom and 82944-atom cells. The temperature corresponds to an instantaneous kinetic energy measurement; the term ''temperature'' is somewhat abusive, as the system is shifted away from equilibrium when the projectile is initially accelerated, but this parameter does constitute a satisfactory indicator of the prevailing agitation inside the simulation cell. Two temperature regimes can be distinguished. The relatively brief first step—a few tenths of a picosecond during which the temperature reaches a plateau situated at about half the initial increase—corresponds to the distribution of the initial kinetic moment of the projectile between excess potential energy and excess kinetic energy. The second step corresponds to a slower drop to room temperature; it is related to the thermal conductivity of the glass medium, and to the system cooling method adopted through control of the outer layer.

The nonlinearity revealed by the atom displacements-versus-energy curve is attributable to the different temperature levels. Room-temperature control of the outer layer of the simulation cell provides for dissipation of the thermal wave when it reaches the cell boundaries, but also results in the penetration of a ''cooling wave'' into the simulation cell. The smaller the cell volume, the sooner the ''cooling wave'' reaches the center of the irradiated zone. The small 5184-atom cells with external room temperature control were thus cooled more quickly than the larger cells, hence the limited number of atom displacements. Although the control is physical in nature (the cells are considered as if they were in direct contact with a room-temperature bath), it introduces a size-related effect to which actual glass wasteforms are not subjected. This effect is not apparent during the initial instants of the cascade, as the depolymerization peak evolves linearly with the energy regardless of the simulation cell dimensions.

In small cells, the larger number of displacements obtained in cascades initiated by uranium atoms than in cascades initiated by oxygen atoms is probably only an artifact, since no comparable difference is observed in larger simulation cells. The denser cascades created by the uranium atoms tend to remain farther from the temperature-controlled zones, hence a potentially greater number of displacements.

In the large-scale cascades, the cooling wave begins to affect the overall temperature only after 1 to 2 ps, and the cell reaches room temperature after a considerably longer time. Since the vast majority of atom displacements occur before the first picosecond, it is reasonable to assume that the slope of the displacement versus energy curve in large simulation cells is not modified by this effect of controlling the outer layer.

From this perspective, a linear increase in the number of displacements with the energy appears to be the rule for cascades in the 1–7 keV energy range in systems with more than 40 000 atoms, and the slope is not disturbed by the outer layer temperature control. The atom displacement density between 3 and 7 keV increases continuously with the number of displacements. Together, these two phenomena suggest that the displacement cascade volume is not a linear function of the energy, but tends to increase at a lower rate at higher energies.

Restoration of the glassy network

All the cascades progress according to the same pattern. The glass structure is first characterized by an intermediate

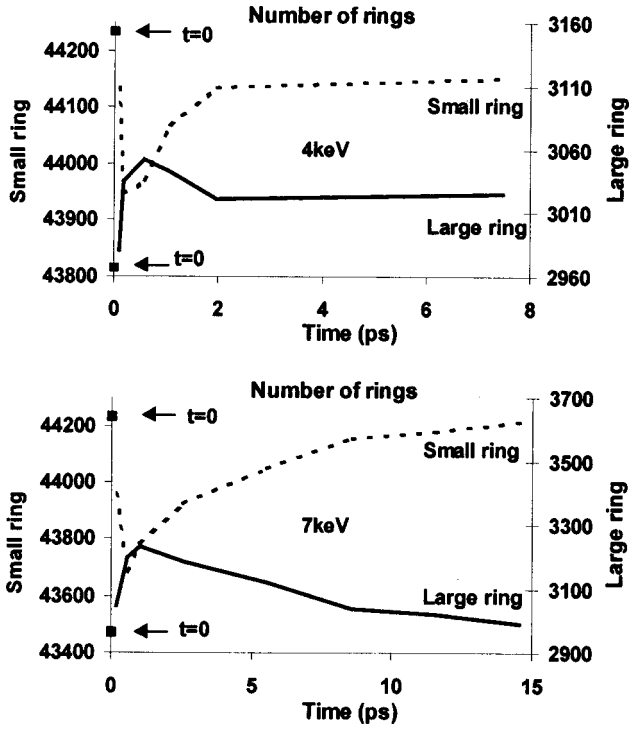

FIG. 16. Number of small rings (containing fewer than five oxygen atoms) and large rings (containing more than six oxygen atoms) versus time for 4 keV and 7 keV cascades in an alkali glass.

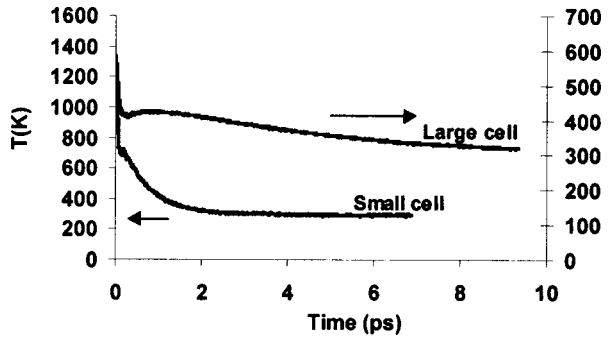

FIG. 17. Temperature versus time during a cascade in 5184-atom and 82944-atom cells.

depolymerization state, the intensity of which increases linearly with the projectile energy, followed by repolymerization with a longer characteristic time. The polymerization of the final structure obtained at the end of this relaxation is never (much) greater than at the outset.

As we said above, the cascade volume increases with a negative curvature versus the energy, it means that the energy density deposited in the core of the cascade increases with the cascade energy. Figure 10 suggests that the final depolymerization versus the cascade energy passes through a maximum for a given simulation cell size and then decreases to zero. If the energy density deposited in the core of the cascade is sufficiently high, all the atomic motions necessary to the structure restoration are thermally activated. This activation energy is clearly lower for alkali glass than for alkali-free glass. When an U atom is accelerated rather than an O atom, the energy density deposited is larger (Fig. 1 shows that the cascades are more dense) and the structure restoration is better (Fig. 10 shows a lower final depolymerization) in agreement with this scheme.

Restoration of the initial structure concerns not only the overall polymerization, but also the concentrations of local groups. The initial structure is reestablished in detail, providing further evidence of the degree of equilibrium in the structures produced by quenching and relaxation as described above under ''Methodology.'' This is an important point with regard to nuclear waste containment, confirming the ease with which the glass withstands atom displacements induced by recoil nuclei, at least at energies up to about 7 keV. The glass structure restoration considered here is an overall restoration of the degree of polymerization, the ring distribution and the mean coordination numbers. During the cascade, however, many atoms did indeed change their equilibrium sites or their local coordination number.

Important features about restoration of the glassy network

The types of oxygen displacements (the most numerous in absolute terms, along with sodium displacements) change as the cascade progresses. The phenomena observed during the initial instants are mainly individual oxygen atom displacements and transitions between the bridging and nonbridging states. As the overall energy diminishes, however, collective displacements and ''break-and-branch'' events become predominant. About 90% of the atom displacements are initiated during the first picosecond, before the glass structure restoration phase. The gradual repolymerization, which requires few additional displacements, occurs through a series of local reorganizations (with no further individual moves). The presence of alkali metals appears to have a major effect in facilitating these reorganizations, as shown by the evolution of the bridging and nonbridging oxygen concentrations (the notion of transition between the bridging and nonbridging states is associated by definition with the presence of alkali metal atoms) during the restoration (Fig. 12). The alkali-enriched zones scattered throughout the glass structure, and the ease with which alkali atoms move and change coordination numbers, provides the glass with a significant degree of freedom that allows each former in the network to find the ideal number of oxygen atoms for its local environment.

In the absence of alkali metals, the borosilicate network remains depolymerized, as the migration of oxygen atoms far from their initial sites cannot be facilitated by alkali species that release or accept an oxygen neighbor as necessary in the local chemistry. The only remaining degree of freedom in the glass is the possible double coordination of boron atoms—and indeed, the depolymerization of $SiO_2+B_2O_3$ structures results in a lower mean coordination number for the boron atoms. Depolymerization in this case does not result from the reconstruction of a more stable structure, since the energy of the structure increases after irradiation: it is indeed poorly restored structural damage due to the limited relaxability of alkali-free glass. These are qualitative observations, that can be decorrelated of the precision with which the potentials are able to reproduce the different chemical interactions. The differences noted in the Introduction between network formers, intermediates and modifiers are reflected in the behavior of the composition during a displacement cascade. A hierarchy appears among the species, with behavior related to the extent of their possible local configurations.

The key to glass irradiation resistance thus appears to lie in the degree of freedom for relaxation arising from the presence of alkali metals and of multicoordinate elements. A systematic investigation of a variety of glass compositions covering a wide transition temperature range (considered here as indicative of the glass relaxability) and irradiated over a significantly broad energy range would be a major undertaking, but would allow more definite conclusions to be drawn concerning this point.

The presence of 3-coordinate aluminum is a methodological artifact: the Al-O potentials used were too low to ensure tetracoordination of all the aluminum atoms. The simultaneous presence of AlO_3 and AlO_4 groups increases the degree of freedom of relaxation, and should logically be expected to accelerate the initial structure restoration.

No conclusion can be drawn from the presence of zirconium oxide because of its low concentration, but the same reasoning as above suggests that increasing the percentage of intermediate species over the network formers would facilitate restoration of the glass structure.

Displacement types

The curves describing the evolution of the different types of displacements and transitions during the 3 keV cascade (Figs. 11, 12 and 14) suggests coupling of the displacements. Over the time interval between 1 and 8 ps, following the depolymerization peak, the shape of the curve is the same for

Na and O displacements, for the number of O_{12} and B_{34} transitions, and for percentage of ''break and branch'' displacements (Fig. 15). Coupling of these processes seems logical, inasmuch as the formation of a BO_4 group requires a nearby alkali metal atom to ensure local electrical neutrality, and the presence of an oxygen atom liable to form an additional chemical bond. The coupling between atom displacements of different species was already revealed during an investigation of the effect of a Coulomb field on the glass structure, and notably the greater mobility of oxygen atoms and network formers made possible by the presence of alkali metal atoms.[23]

The observed delay in the displacement of alkali metal atoms was the subject of an earlier study[23] in which several examples were discussed of the lower probability for alkali atoms to be involved in a violent collision because of their location in regions of lower atom density. Their peripheral position around the disturbed regions could be an energy-related phenomenon. Collective movements and break-and-branch phenomena are the least costly displacements in energy terms, and become increasingly numerous as the system energy diminishes—i.e., as the collision progresses toward the periphery of the damage zones. These displacement modes are coupled with those of the alkali metals.[23] Together, the collective displacements around the periphery and the facilitation by the alkali metals account for the ring of displaced alkali atoms around the edges of the damage zones.

Anticipation about segregation and point defects annealing

Glass restoration without long-range displacements limits the risk of segregation in the structure, particularly since the high-energy phase responsible for atom displacements further limits segregation phenomena by virtue of the random displacement directions.

Interaction potentials based on formal ion charges cannot represent possible point defects (peroxy radicals, E' centers) for instability reasons. In semiconductors and pure metals, a displacement cascade results in a distribution of (interstitial and vacancy) point defects for which recombination is closely related to the medium range atom mobility, which in turn is correlated with the ratio between the local temperature induced by the projectile and the material melting temperature. In complex oxide glasses, the topologies of point defects (whose absence is obviously detrimental to the physical realism of the simulations) are such that long-range atom displacements are unnecessary to eliminate them, given the possibilities for local rearrangements. Here again, it can be expected that the many local configurations in a complex glass will tend to enhance its resistance to the accumulation of point defects.

What a phenomenological model could be

The fractionation of the damage zones by the initial projectile seems to be a common but nonsystematic characteristic, with no clear relation to the energy involved. At constant energy, the damage zones may be fractionated or homogeneous; the energy and localization of the few violent collisions during the high-energy phase determine the final perturbation morphology. This is a highly chaotic process depending on the initial projectile direction and on the instantaneous atom positions; only statistical laws determined from a larger number of examples can be considered reliable. Nevertheless, increasing the projectile energy not only increases the length of the path and should thus favor fractionation, but also increases the volume of the individual damage zones, which eventually overlap and tend toward greater morphological homogeneity. These two concurrent mechanisms make it difficult to extrapolate the cascade morphology to higher energies. However, the example of ordered systems shows the existence of a threshold above which the probability of generating subcascades approaches 1, ensuring a fractionated defect distribution; it would be surprising if a fractionation threshold could not be defined for even complex glasses.

In order to address the issues of complete nuclear glasses subjected to α-decay recoil nuclei, the currently available results must be extrapolated to higher energies and to more complex compositions. An important aspect highlighted in this article concerns the distribution of depolymerization peaks in the damage zones. The first zones affected are subjected to a depolymerization peak that tends to saturate when the projectile energy increases, while in the more remote zones the depolymerization peaks continue to rise. These observations could provide guidelines for developing a more global model in which displacement cascade morphologies are described as a group of individual zones, each subjected to a depolymerization peak that cannot exceed a volume-dependent saturation level, and sustaining thermal annealing that could be described by the projectile path and the thermal conductivity of the material.

Discussion related to TRIM calculations and displacement energies

The TRIM or MARLOWE codes[24,25] could be used to extend the computer-dependent energy limit by approximating the cascade morphology at actual energies, particularly since the number of displacements calculated by the TRIM code is consistent with the number of individual displacements obtained in molecular dynamics.[2] The TRIM code was used to simulate 4 MeV oxygen atoms irradiating a glass with the same composition as the alkali-borosilicate glass studied here, yielding a total of about 750 atom displacements (defined as the number of atoms receiving an energy exceeding the displacement energy). The energy (4 MeV) lost by the oxygen atoms corresponds to 45 keV lost during atomic collisions. The multiple displacement modes cannot be reproduced by a binary collision model; a molecular dynamics simulation by extrapolating the number-of-displacements-versus-energy line therefore results in about 30 000 displacements. However, if it is assumed that 5% on average of these displacements correspond to individual moves (as taken into account by the TRIM code), the result is on the same order of magnitude as the number obtained from a binary collision approach.

Applying the Kinchin-Pease model directly based on the total number of displacements yields low displacement energy values; this, however, merely highlights the fact that the model is inapplicable to complex vitreous structures. We checked that the individual displacement energies obtained by displacing one atom from its equilibrium site are on the order of 40 eV on average in agreement with conventional

values. This is an important point in that it shows that the potential model used realistically represents atom displacements. During a cascade, however, the actual displacement distance distribution varies continuously from 0 to the maximum distance, so that defining a ''displacement'' is not a simple problem. We opted for an empirical definition capable of visualizing the positions of the atoms displaced over the greatest distances, and thus of visualizing the zones of greatest disturbance. This definition includes not only displacements due to ballistic collisions, but also collective movements accompanying ballistic collisions and diffusive movements in the local liquid region that forms temporarily in the midst of the cascade. The very nature of the vitreous network itself, comprising a polymerized network mixed with highly mobile regions, implies that collective displacements tend to predominate. The Kinchin-Pease model, which takes only ballistic collisions into account, is not applicable in this framework.

Volume change

Another systematically observed feature concerns volume or pressure changes in the cells after a cascade: the cell volume was always either unchanged or increased; no significant contraction was ever observed. Considering the results presented in this paper, it is difficult to propose a single explanation for this expansion, although a number of significant coincidences may be noted. In glasses without alkali metals, expansion was always associated with transitions between BO_4 and larger BO_3 groups with the exception of a single case in which extensive depolymerization occurred without expansion. An increase in the number of 3-coordinate boron atoms is thus not systematically coupled with cell expansion. The two cascades that produced the greatest swelling in the alkali glasses resulted in an increase in the Voronoï volumes around boron and alkali metal atoms. The phenomenon may be attributed to swelling of alkali-rich regions or to swelling due to poorer overall reconstruction of BO_4 groups (whose local neutrality requires the presence of an alkali) at the end of the cascade. The latter explanation accounts for the simultaneous variations in the boron and alkali environments.

Finally, in cascades with energies above 3 keV, the higher number of large rings is clearly correlated with the magnitude of the expansion, although this correlation is not obvious in the case of lower energy cascades in the 5184-atom systems. The increase is due to rapid annealing after the thermal peak, which ''freezes'' the local structural changes. Cell expansion following irradiation can thus be explained by one or more possible causes. The result clearly observed during the first calculations on glasses containing CaO in addition to Na_2O (Ref. 26) (i.e., expansion of the alkali-rich regions and reordering of the polymerized network) cannot be confirmed by the latest calculations; the first observations may have been due to incomplete relaxation of the initial structure.

The experimental findings also indicate systematic swelling of alkali-borosilicate glasses under α irradiation in proportions close to those observed here, although the mechanism remains to be identified (swelling of alkali-rich regions? modification of the polymerized network? creation of bubbles or point defects?). The present simulations merely suggest that the swelling may be due exclusively to modification of the glass network, without necessarily giving rise to new entities.

CONCLUSIONS

A molecular dynamics study of displacement cascades at energies ranging from 300 eV to 7 keV in glass compositions with and without alkali metals revealed the influence of the latter on the thoroughness of structural restoration. More generally, following a depolymerization peak, the glass structure is reconstructed by local readjustments, facilitated by the presence of alkali metal atoms. If the cascade energy is sufficiently high, the initial structure is completely restored. This means that despite the many atom displacements and local coordination changes, the degree of polymerization, the mean coordination numbers and the ring distributions are conserved. About 90% of the atom displacements occur during the first instants of the cascade, during the thermal peak; displacements during the initial structure restoration phase account for only a small fraction of the total.

Several types of displacements were identified, ranging from jumps by individual atoms to collective displacements of an atom and its neighbors. Individual displacements and $O_{bridging}$-$O_{nonbridging}$ transitions were the most numerous during the first instants of the cascade, but were quickly superseded by collective displacements and local break-and-rebranch processes.

The structure volume was observed to remain stable or increase after irradiation, but never to diminish. Coincidental evidence was noted between the coordination numbers, the ring size distributions, the Voronoï volumes and the cell expansion, but no single comprehensive explanation is forthcoming.

Finally, we observe that nuclear glasses easily accommodate displacements cascades, and this is an important result in regard of the long term storage of the oxide matrices.

ACKNOWLEDGMENTS

The authors are grateful to Y. Serruys and K. Abbas for the TRIM code results and to J.-P. Crocombette for a constructive critical reading of this paper. COGEMA is also thanked for his financial support.

[1] Hj. Matzke and E. Vernaz, J. Nucl. Mater. **201**, 295 (1993).
[2] W. J. Weber, R. C. Ewing, C. A. Angell, G. W. Arnold, A. N. Cormack, J.-M. Delaye, D. L. Griscom, L. W. Hobbs, A. Navrotsky, D. L. Price, A. M. Stoneham, and M. C. Weinberg, J. Mater. Res. **12**, 1946 (1997).
[3] M. T. Robinson, J. Nucl. Mater. **216**, 1 (1994).
[4] K. Nordlund and R. S. Averback, Phys. Rev. B **56**, 2421 (1997).
[5] T. K. Chaki and J. C. M. Li, Philos. Mag. B **51**, 557 (1985).
[6] N. V. Doan, Philos. Mag. A **49**, 683 (1984).
[7] K. Nordlund, M. Ghaly, R. S. Averback, M. Caturla, T. Diaz de la Rubia, and J. Tarus, Phys. Rev. B **57**, 7556 (1998).
[8] D. C. Rapaport, *The Art of Molecular Dynamics* (Cambridge University Press, Cambridge, England, 1995).
[9] H. Scholze, *Glass: Nature, Structure and Properties* (Springer, Berlin, 1991).
[10] W. H. Zachariasen, J. Am. Chem. Soc. **54**, 3841 (1932).
[11] D. Ghaleb, J.-L. Dussossoy, C. Fillet, F. Pacaud, and N. Jacquet-Francillon, in *Scientific Basis for Nuclear Waste Management XVIII*, edited by T. Murakami and R. C. Ewing, MRS Symposia Proceedings No. 353 (Materials Research Society, Warrendale, PA, 1995), p. 107.
[12] H. C. Andersen, J. Chem. Phys. **72**, 2384 (1980).
[13] F. H. Stillinger and T. A. Weber, Phys. Rev. B **31**, 5262 (1985).
[14] B. P. Feuston and S. H. Garofalini, J. Chem. Phys. **89**, 5818 (1988).
[15] J.-M. Delaye and D. Ghaleb, J. Non-Cryst. Solids **19**, 5239 (1996).
[16] J.-M. Delaye, V. Louis-Achille, and D. Ghaleb, J. Non-Cryst. Solids **210**, 232 (1997).
[17] J. F. Ziegler, J. P. Biersack, and U. Littmark, *The Stopping and Range of Ions in Matter* (Pergamon, New York, 1985).
[18] T. F. Soules and A. K. Varshneya, J. Am. Ceram. Soc. **64**, 145 (1981).
[19] T. F. Soules and R. F. Busbey, J. Chem. Phys. **78**, 6307 (1983).
[20] P. Vashishta, P. Kalia, and R. J. Rino, Phys. Rev. B **41**, 12 197 (1990).
[21] P. J. D. Lindan and M. J. Gillan, J. Phys. Condens. Matter **3**, 3929 (1991).
[22] N. V. Doan and F. Rossi, Solid State Phenom. **30&31**, 75 (1993).
[23] J.-M. Delaye and D. Ghaleb, Nucl. Instrum. Methods Phys. Res. B **135**, 201 (1998).
[24] J. P. Biersack, Radiat. Eff. Defects Solids **129**, 15 (1994).
[25] M. T. Robinson, Phys. Rev. B **40**, 10 717 (1989).
[26] J.-M. Delaye and D. Ghaleb, Nucl. Instrum. Methods Phys. Res. B **153**, 157 (1999).